Adhesion paradox: Why adhesion is usually not observed for macroscopic solids

A. Tiwari [1,*] J. Wang [1,2] and B. N. J. Persson [1,*]
[1]*PGI-1, FZ Jülich, Germany, Jülich 52428, European Union*
[2]*College of Science, Zhongyuan University of Technology, Zhengzhou 450007, China*

The adhesion paradox refers to the observation that for most solid objects no adhesion can be detected when they are separated from a state of molecular contact. The adhesion paradox results from surface roughness, and we present experimental and theoretical results that show that adhesion in most cases is "killed" by the longest-wavelength roughness. In addition, adhesion experiments between a human finger and a clean glass plate were carried out, and for a dry finger no macroscopic adhesion occurred. We suggest that the observed decrease in the contact area with increasing shear force results from nonadhesive finger-glass contact mechanics, involving large deformations of complex layered material.

I. INTRODUCTION

All solids have surface roughness extending over many decades in length scale, which has a large influence on most tribology topics, such as adhesion, boundary and mixed lubrication, and the leakage of seals. Surface roughness is the main reason why macroscopic solid objects usually do not adhere to each other, despite the strong force fields that act at the atomic length scale between all atoms; this is referred to as the adhesion paradox [1]. Strong adhesion between two macroscopic objects is observed only if both solids have very smooth surfaces, or if at least one of the solids is elastically very soft. In Nature, insects, lizards, and tree frogs have "learned" (via natural selection) how to construct soft adhesion pads from stiff materials using hierarchical building principles [2,3].

In this paper, we address two topics that have recently been discussed controversially in the literature [4–8]. We first present experimental and theoretical results showing that adhesion is "killed" mainly by the longest-wavelength roughness. This is the reason why small particles may adhere strongly (agglomerate), while macroscopic solids of the same material may show no adhesion during approach or separation. We also present experimental results for adhesion between a human finger and a glass plate, which is relevant for haptic applications [9,10].

II. EXPERIMENT

A. Sandblasting and surface topography

We have sandblasted two polymethylmethacrylate (PMMA) sheets with glass beads (spherical particles with smooth surfaces) of diameter ≈ 10 μm for a time ranging from 1 to 4 min using 5–8 bar air pressure. The topography measurements were performed with a Mitutoyo Portable Surface Roughness Measurement device, Surftest SJ-410,

with a diamond tip with a radius of curvature $R = 1$ μm, and with the tip-substrate repulsive force $F_N = 0.75$ mN. The lateral tip speed was $v = 50$ μm/s. In the applications presented below, the radius of curvature of the tip was always smaller than the surface curvature radius, which is a necessary condition for reliable measurements of surface topography [11].

Surface topography is often studied using optical methods, e.g., confocal microscopy. However, we have had a bad experience with optical methods. Thus they may reproduce the long-wavelength roughness correctly, but often not the shorter-wavelength part (and they often give a high fraction of undefined points). For this reason, we use an engineering stylus instrument and atomic force microscopy for the short-wavelength region if necessary.

From the measured surface topography (line scans), $z = h(x)$, we calculated the one-dimensional (1D) surface roughness power spectra defined by

$$C_{1D}(q) = \frac{1}{2\pi} \int dx \langle h(x)h(0)\rangle e^{iqx},$$

where $\langle \cdots \rangle$ stands for ensemble averaging. For surfaces with isotropic roughness, the two dimensional (2D) power spectrum $C(q)$ can be obtained directly from $C_{1D}(q)$ as described elsewhere [12,13]. For randomly rough surfaces, all the (ensemble-averaged) information about the surface is contained in the power spectrum $C(q)$. For this reason, the only information about the surface roughness that enters in (analytic) contact mechanics theories (with or without adhesion) is the function $C(q)$.

B. Replicating roughness of PMMA on PDMS

The sandblasted PMMA surfaces were cleaned with distilled water and then dried. We produced elastomer replicas of the two rough surfaces, and a smooth PMMA surface, using Sylgard 184 Polydimethylsiloxane (PDMS) obtained from Dow Corning. This elastomer is obtained from two
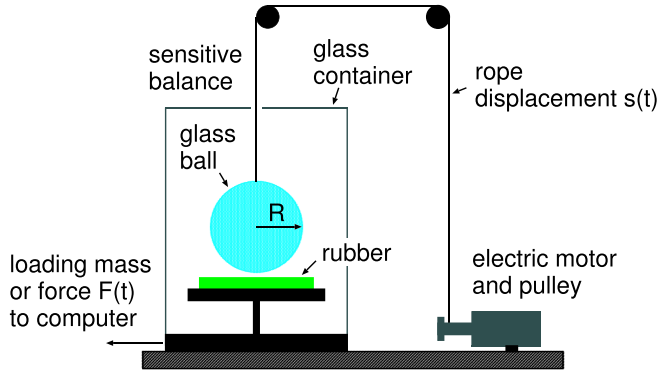
FIG. 1. The Jülich experimental setup for measuring adhesion.

liquid components, namely a prepolymer base, B, and a cross-linking agent, C. The two components can be mixed in varying ratios to obtain desired elastic properties. For our purpose, we prepared PDMS by choosing a C:B ratio of 1:10. We poured the PDMS fluid on the smooth and sandblasted PMMA surfaces and kept it on a heated plate maintained at $70\,°C$ for 24 h. After this curing process, we slowly removed the (1-cm-thick) PDMS sheets from the PMMA surfaces. It has been shown in the past that PDMS can replicate roughness down to the nanoscale [14,15].

C. Adhesion measurement

We have studied the adhesion interaction between a spherical glass ball (diameter $2R = 2.5$ cm) and PDMS rubber sheets. In the experiments, we brought a glass ball into contact with a rubber substrate as shown in Fig. 1. The rubber sample is positioned on a very accurate balance (analytic balance produced by Mettler Toledo, model MS104TS/00), which has a sensitivity of 0.1 mg (or $\approx 1\ \mu N$). After zeroing the scale of the instrument, we can measure the force on the substrate as a function of time, which is directly transferred to a computer at a rate of 10 data points per second.

To move the glass ball up and down, we have used an electric motor coiling up a nylon cord, which is attached to the glass ball. The pulling velocity as a function of time can be specified on a computer. In the experiments reported further below, the glass ball is repeatedly moved up and down with the speed 5 μm/s for up to ~25 contact cycles, involving a measurement time of up to 20 h.

The adhesion between a human finger and a smooth glass plate in a dry state was studied in the setup described above by application of $\approx$0.6 N force nominally on the smooth glass plate by the finger and then slowly removing the finger away from the glass plate. The glass plate was cleaned with acetone and isopropanol, and the human finger of one of the authors was cleaned with soap and water before each experiment. For adhesion in water, a drop of water was placed on the glass plate, and then the same procedure was repeated as for the dry state.

III. ROLE OF SURFACE ROUGHNESS AT DIFFERENT LENGTH SCALES ON ADHESION

Due to the surface roughness, which exists on all solid objects, adhesion between macroscopic solid bodies is usually not observed. This is because to make contact, the solids must deform at the contacting interface, and this stores up elastic energy at the interface that is given back during the separation of the solids and helps to break the atomic bonds at the contacting interface. The elastic energy required to bend the surface of a solid (with Young's elastic modulus E) so that it fills out a cavity of width λ and depth $h << \lambda$ is of order $E_{el} \approx \lambda^3 E(h/\lambda)^2 = \lambda h^2 E$, while the gain in adhesion energy is $E_{ad} \approx \lambda^2 \Delta\gamma$, where $\Delta\gamma$ is the work of adhesion (the energy per unit surface area to separate two flat surfaces of the two materials involved). Here we have used that the elastic strain $\epsilon \approx h/\lambda$ and that the deformation field extends over a volume $\approx \lambda^3$. The ratio $E_{el}/E_{ad} = (E/\Delta\gamma)(h^2/\lambda)$. If we consider cavities of different sizes but with the same ratio h/λ, then $E_{el}/E_{ad} \sim \lambda$, i.e., the elastic energy will dominate over the adhesive energy at large enough length scales λ. The same holds more generally for self-affine fractal surfaces with the fractal dimension $D_f < 2.5$. In fact, in Ref. [16] it was shown that for full contact the elastic energy is dominated by the long-wavelength roughness components for $D_f < 2.5$, and by short-wavelength components for $D_f > 2.5$. However, most real surfaces have $D_f < 2.5$ (see Ref. [20]), and the elastic energy will dominate over the adhesive part for large enough length scales. This is the basic reason adhesion is not observed in most cases for macroscopic solids even if adhesion may be strong for small solid objects (e.g., nanoparticles) of the same material [16–18]. It is the reason why small particles may agglomerate into bigger particles, while macroscopic bodies made from the same materials may not adhere at all. Here we will present experimental results and calculations illustrating this fundamental conclusion.

A. Experimental results

We have produced (nearly) randomly rough polymethyl-methacrylate (PMMA) surfaces using sandblasting. From theories of growth (or here erosion) one expects the root-mean-square (rms) roughness to increase continuously with the sandblasting time, with a roll-off in the surface power spectrum that is moving to longer wavelength (shorter wave number) with increasing sandblasting time [19,20]. Thus the theory predicts that the short-wavelength roughness is independent of the sandblasting time, while more longer-wavelength roughness is added with increasing sandblasting time. We have observed the same effect by varying the kinetic energy of the sandblasting particles.

The green, red, and blue lines in Fig. 2 show the wave-number dependency of the 1D surface roughness power spectra for a smooth PMMA surface, and two sandblasted surfaces (denoted 1 and 2), respectively (log-log scale). The surface 1 was sandblasted for 4 min using 5 bar air pressure, and the surface 2 for 1 min using 8 bar air pressure. Note that the large wave-number (short-wavelength) power spectra of the two sandblasted surfaces are the same, while for small wave number the surface 2 has a larger power spectrum, which
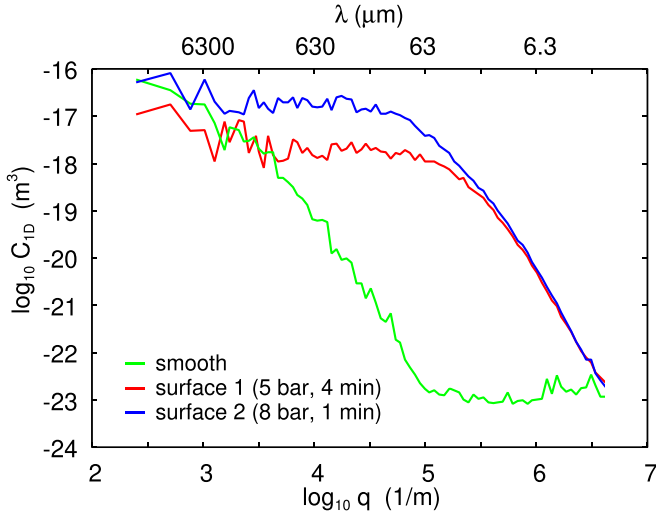
FIG. 2. The green, red, and blue lines shows the wave number q (and wavelength $\lambda = 2\pi/q$) dependency of the 1D surface roughness power spectra for the smooth, sandblasted 1, and sandblasted 2 surfaces, respectively (log-log scale).

is reflected in the rms-roughness amplitude, which is 0.78 and 1.73 μm for surfaces 1 and 2, respectively. The rms-slope is determined mainly by the short-wavelength roughness and is nearly the same (0.18 and 0.22, respectively). The rms-slope of the smooth surface is much smaller, 0.04.

Using the adhesion setup described in Sec. II, we have measured the pull-off force between the glass ball and the smooth and rough (surfaces 1 and 2) PDMS rubber surfaces. Figure 3 shows the interaction force between the glass ball and the three PDMS surfaces during one contact. The green, red, and blue lines are for the smooth, sandblasted 1, and sandblasted 2 surfaces, respectively. Note that no adhesion can be detected on approach for any of the surfaces, and for the sandblasted 2 surface also not during pull-off (retraction).
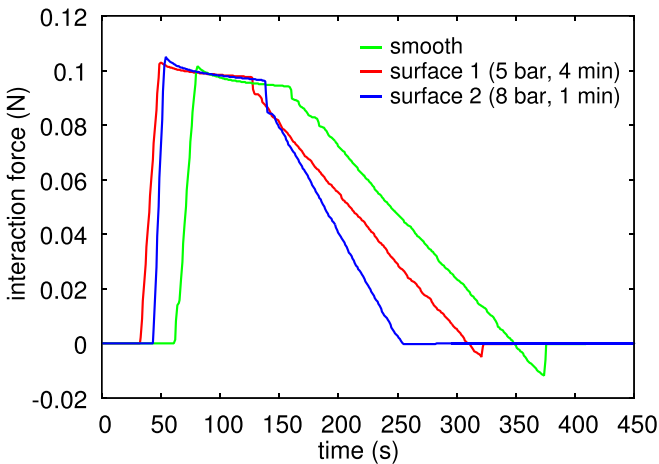

FIG. 3. The interaction force between the glass ball and the three PDMS surfaces. The green, red, and blue lines are for the smooth, sandblasted 1, and sandblasted 2 surfaces, respectively. Note that no adhesion can be detected on approach, and for the sandblasted 2 surface also not during pull-off (retraction).
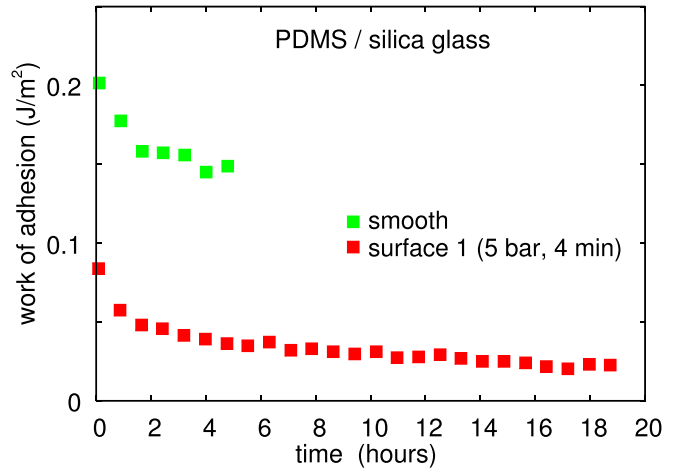

FIG. 4. The work of adhesion as a function of time, where each data point is obtained from the pull-off force in each sequential contact cycles. Here, we show data for the smooth PDMS surface (green squares) and for the PDMS replica of the sandblasted surface 1 (red squares).

That is, the additional long-wavelength roughness of the surface 2 as compared to the surface 1 has killed the macroscopic adhesion, while surface 1 shows a pull-off force roughly half as large as that for the smooth PDMS surface.

Using the Johnson-Kendall-Roberts (JKR) theory, from the pull-off force F_c we can obtain the work of adhesion,

$$F_c = \frac{3\pi}{2}\gamma R.$$

In Fig. 4 we show the work of adhesion γ to separate the surfaces as a function of the number of contacts for the smooth PDMS surface (green squares) and the sandblasted surface 1 (red squares). For surface 2 the work of adhesion to separate the surfaces vanishes. The work of adhesion during approach (contact formation) vanishes for all three surfaces, i.e., strong contact hysteresis occurs in all cases. Note also that the work of adhesion to separate the surfaces drops with the number of contacts, which we attribute to the transfer of un-cross-linked molecules from the PDMS to the glass ball, which has been observed also for other rubber compounds [17,21,22].

B. Theory results

The two rough PDMS surfaces used above have large roll-off regions, which have a small influence on the adhesion. We therefore first illustrate the role of different length scales on adhesion with a case without a roll-off region. We consider a self-affine fractal surface with the fractal dimension 2, which implies that the ratio between the amplitude and the wavelength is the same independent of the wavelength of the roughness component. Thus on a log-log scale the 2D power spectra as a function of the wave number is a straight line with slope -4 (see Ref. [3]). We assume the small and large cutoff wave numbers $q_0 = 10^4$ m^{-1} and $q_1 = 10^9$ m^{-1}. The surface has rms-roughness 10 μm and rms-slope 0.48.

Figure 5 shows the effective interfacial binding energy (per unit surface area), or work of adhesion, as a function of the magnification (lower scale) or the wave number (upper
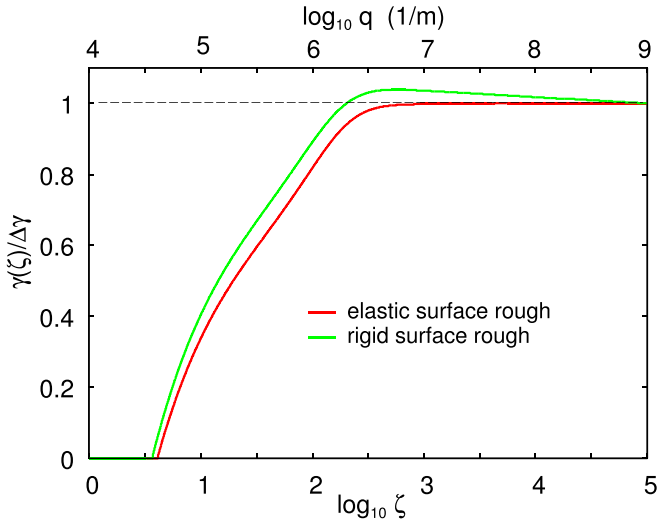
FIG. 5. The calculated effective interfacial binding energy (per unit surface area), or work of adhesion, as a function of the magnification (lower scale) or the wave number (upper scale). Note that $\gamma(\zeta)$ at the magnification ζ is the interfacial binding energy including only the roughness components with $q > \zeta q_0$ (where q_0 is the smallest wave number). The red and green line is for the roughness on the elastic solid and rigid solid, respectively. In the calculation we used $\Delta\gamma = 0.1 \text{ J/m}^2$ and $E^* = 1.0 \text{ MPa}$.

scale). Note that $\gamma(\zeta)$ at the magnification ζ is the interfacial binding energy including only the roughness components with $q > \zeta q_0$ (where q_0 is the smallest wave number). The red and green lines are for the roughness on the elastic solid and on the rigid solid, respectively. In the present case, $\gamma(\zeta)$ vanishes before reaching $\zeta = 1$, i.e., there is no macroscopic pull-off force for either case. Note that the drop in $\gamma(\zeta)$ is due to the longer-wavelength part of the roughness spectra. In fact, for the case in which the roughness occurs on the rigid surface, the short-wavelength part of the roughness spectra enhances the work of adhesion $\gamma(\zeta)$ for large ζ. This effect is due to the increase in the surface area (we have assumed that the interfacial binding energy per unit surface area is unchanged by the increase in the surface area, which may hold for rubberlike materials as they have a thin surface layer with liquidlike mobility).

Since there is no macroscopic adhesion, $\gamma(1) = 0$, the contact area will vanishes continuously as the applied nominal contact pressure approaches zero. This is shown in Fig. 6. The figure shows the projected area of real contact A, normalized by the nominal contact area A_0, as a function of the nominal applied (squeezing) pressure. The red and green lines are for the roughness on the elastic solid and the rigid solid, respectively. When macroscopic adhesion occurs, i.e., $\gamma(1) > 0$, the area of real contact is nonzero also when the applied pressure vanishes. See Ref. [23–25] for results illustrating this.

Note that even if the macroscopic adhesion vanishes (no pull-off force), the area of real contact is increased by the adhesion. This implies, for example, that the adhesive interaction will increase the sliding friction force even if no adhesion can be detected in a pull-off experiment.

Next, let us consider the work of adhesion between the silica glass ball and the smooth and rough PDMS surfaces
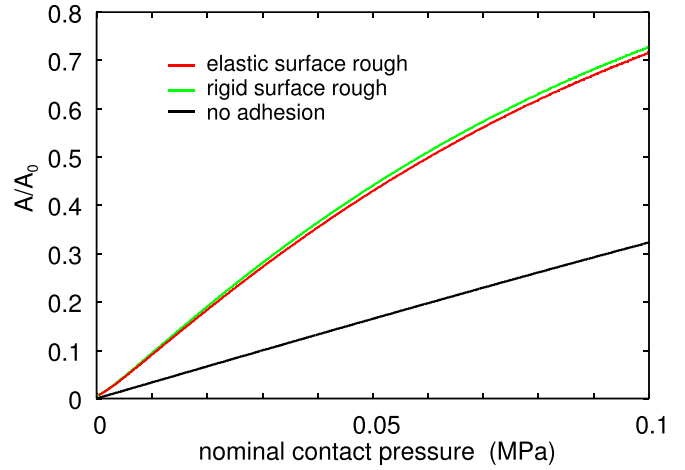
studied above. From the 1D surface roughness power spectra shown in Fig. 2, we first calculated the 2D surface roughness power spectra shown in Fig. 7. Using the Persson contact mechanics theory [24], in Fig. 8 we show the calculated effective interfacial binding energy (per unit surface area), or work of adhesion, as a function of the magnification (lower scale) or the wave number (upper scale). In the calculation, we have used the low-wave-number cutoff q_0 indicated by the dashed vertical line in Fig. 7. We have chosen $q_0 \approx 2\pi/r_0$, where $r_0 \approx 0.38$ mm is the JKR radius of the circular contact region at the point of snap-off for the PDMS surface 1. The green, red, and blue lines are for the smooth, sandblasted 1, and sandblasted 2 surfaces, respectively. For the smooth PDMS surface there is a negligible influence of the surface roughness,

FIG. 6. The projected area of real contact A, normalized by the nominal contact area A_0, as a function of the nominal applied (squeezing) pressure. The red and green lines are for the roughness on the elastic solid and rigid solid, respectively. The black line is the result without adhesion.
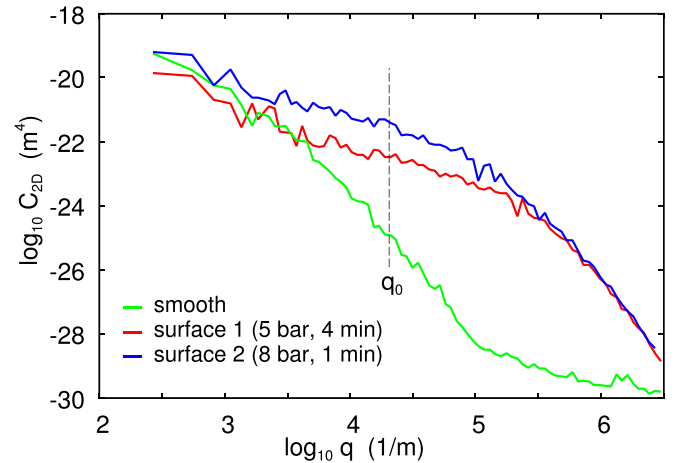

FIG. 7. The green, red, and blue lines shows the wave-number dependency of the 2D surface roughness power spectra for the smooth, sandblasted 1, and sandblasted 2 surfaces, respectively (log-log scale). The dashed vertical line indicates the lower cutoff wave number used in the adhesion calculations.
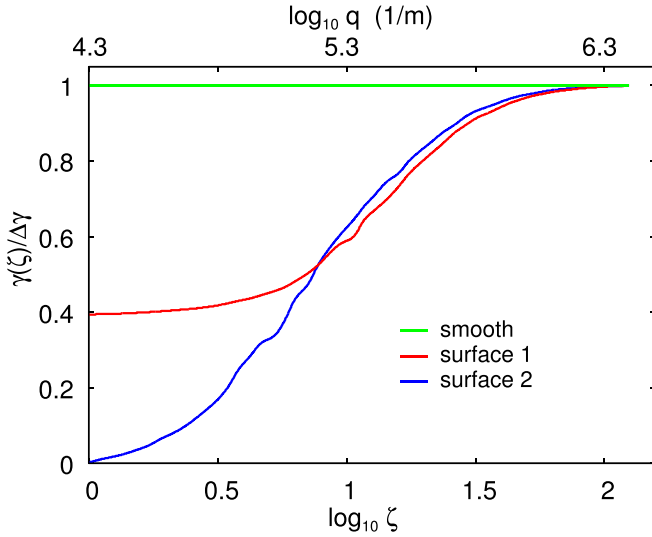
FIG. 8. The effective interfacial binding energy (per unit surface area), or work of adhesion, as a function of the magnification (lower scale) or the wave number (upper scale). Note that $\gamma(\zeta)$ at the magnification ζ is the interfacial binding energy including only the roughness components with $q > \zeta q_0$ (where q_0 is the smallest wave number). The green, red, and blue lines are for the smooth, sand-blasted 1, and sandblasted 2 surfaces, respectively. In the calculation we used $\Delta\gamma = 0.2 \, \text{J/m}^2$ and $E = 2.3$ MPa, $\nu = 0.5$.

so the work of adhesion ($\gamma \approx 0.201 \, \text{J/m}^2$ for the first contact in Fig. 4) should be the same as for perfectly smooth surfaces.

For the surface 2 we predict vanishing macroscopic ($\zeta = 1$) interfacial binding energy, which is consistent with the experimental observation of vanishing pull-off force from this surface. For surface 1 we get $\gamma(1)/\Delta\gamma \approx 0.4$, which is close to the observed work of adhesion ratio for the first contact $\approx 0.083/0.201 \approx 0.413$ (see Fig. 4).

In Ref. [4], Pastewka and Robbins deduced a criterion for strong adhesion that depends on the surface roughness only via the surface rms-slope h' and the rms-curvature h''. These quantities are determined mainly by the shortest-wavelength roughness, corresponding to the largest-wave-number region of the surface roughness power spectrum $C(q)$. This conclusion is opposite to what we have found above and in previous studies [16,23–25]. In fact, for the contact between a soft solid (e.g., rubber) and a stiff solid (e.g., silica glass), if the surface roughness occurs on the stiff solid, then the short-wavelength roughness may even enhance the macroscopic adhesion by increasing the area of real contact (see Refs. [23,24]).

The fundamental reason why the long-wavelength roughness often kills the adhesion (as found above for surface 2) is that it costs a lot of energy to deform the solids at a large length scale. Thus one can show that the ratio between the elastic deformation energy and the interfacial binding energy, assuming perfect contact between an elastic solid with surface roughness and a rigid flat surface, is [16]

$$\frac{U_{\text{el}}}{U_{\text{ad}}} = \frac{E^*}{\Delta\gamma} \frac{\pi}{2} \int_{q_0}^{q_1} dq \, q^2 C(q),$$

where $E^* = E/(1 - \nu^2)$. For a self-affine fractal surface $C \sim q^{-2(1+H)}$ we get

$$\frac{U_{\text{el}}}{U_{\text{ad}}} \sim \frac{E^*}{\Delta\gamma} \int_{q_0}^{q_1} dq \, q^{-2H}.$$

Since typically $H \approx 0.7$–1, it is clear from this equation that the small-wave-number region ($q \approx q_0$) of the power spectrum will give a much larger contribution to the integral than the large-wave-number region ($q \approx q_1$).

The small-wave-number cutoff $q_0 \approx 2\pi/r_0$ is determined by the radius r_0 of the ball-flat contact region at snap-off. If this is in the roll-off region of the roughness power spectrum, then the result is not sensitive to the exact value of r_0. If r_0 occurs in the region where the surface roughness shows self-affine fractal scaling, then one needs to know r_0 relatively accurately either from experiment or from the JKR theory. (It can be iteratively obtained from the JKR theory; first one assumes a reasonable r_0 and calculates the work of adhesion γ and then uses γ in the JKR theory to obtain a new r_0 at pull-off, and so on.)

We note that when a roll-off occurs in the power spectrum, most of the roll-off region is not very important for the macroscopic adhesion, but most important (if r_0 is in the roll-off region) is the long-wavelength roughness just before entering the roll-off region.

Finally, we note that if long-range interactions occur between the solids, adhesion will always be observed independent of the magnitude of the surface roughness. This is the case for capillary bridges between hydrophilic surfaces (assuming enough fluid) and for electrostatic interactions, e.g., due to charging or an applied voltage as in electroadhesion. However, for short-ranged interactions such as chemical or physisorption (van der Waals) bonds, surface roughness can kill adhesion.

IV. FINGER-GLASS ADHESION EXPERIMENTS

Several recent experimental studies have shown that when a tangential force is applied to a human finger squeezed against a flat glass surface, the glass-finger nominal contact area decreases [5,10]. This has been tentatively explained using the adhesion theory described in Ref. [26]. However, we have performed adhesion experiments for a finger in contact with a glass plate, and for a dry finger we do not observe any macroscopic adhesion, so the explanation proposed in Ref. [26] cannot explain the observed decrease in the contact area with increasing tangential force.

Figure 9 shows the interaction force between a human finger and a dry glass plate cleaned by acetone and isopropanol. Case (a) (red curve) is for a not cleaned finger, (b) (green curve) for a finger cleaned with soap and water, and (c) (blue curve) for a clean wet finger. In cases (a) and (b), no (macroscopic) adhesion is observed, while in case (c) we do observe adhesion with a pull-off force $F_c \approx 5.5$ mN. This is similar to what is expected if a capillary bridge is formed between the glass surface and the finger. Thus for a thick water film $F_c \approx 4\pi R\gamma_w$, where the water surface tension $\gamma_w \approx 0.07 \, \text{J/m}^2$, and R is the radius of curvature of the finger. If we use $R \approx 0.7$ cm we obtain the observed pull-off force. However, the pull-off force depends on the volume of water on the finger, and if the
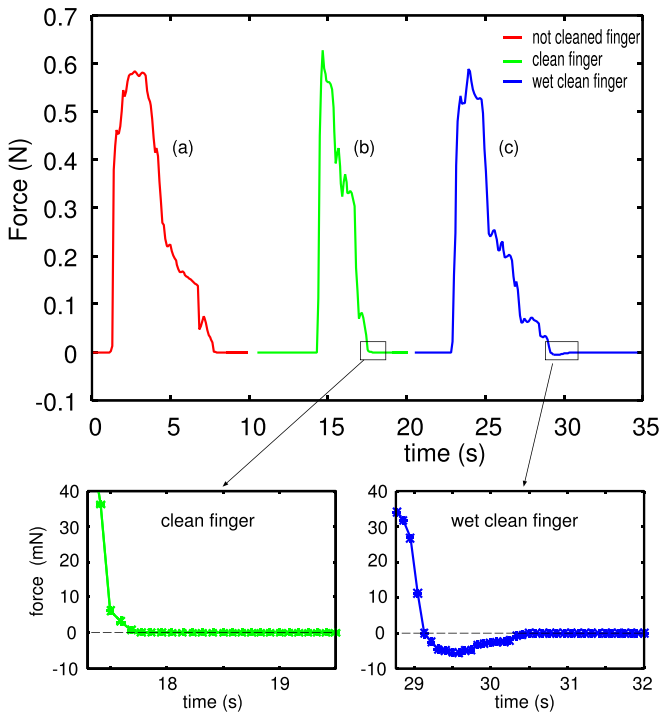
FIG. 9. The interaction force between a human finger and a dry glass plate cleaned by acetone and isopropanol. Case (a) (red curve) is for a not cleaned finger, (b) (green curve) for a finger cleaned with soap and water, and (c) (blue curve) for a clean wet finger. In cases (a) and (b), no (macroscopic) adhesion is observed, while in case (c) do we observe adhesion with a pull-off force $F_c \approx 5.5$ mN. The results are qualitatively the same for different fingers on different persons. The glass surface is very smooth (rms roughness ≈ 20 nm when measured over 1 mm line track). The finger roughness was not studied, but other studies (see Ref. [27]) have shown the roughness amplitude to be of order 0.1 mm, thus (as expected) much larger than that of the glass plate.

water volume is too small (less than ~ 1 mm^3) no adhesion is observed, which we interpret as resulting from the skin surface roughness and the elastic rebound of the deformed skin.

We did not perform a theoretical analysis of the finger-glass contact problem because of the complex nature of the problem (layered viscoelastic material, with material properties sensitive to water and the relative humidity).

We believe that the reduction in the contact area observed for the human finger with increasing lateral force is due to the complex inhomogeneous (layered) nature of the finger and the large deformations involved. It is also possible that the superposition of the normal and parallel deformation fields assumed in most analytic treatments is not accurate enough when the parallel deformations become large and coupling effects become important. This conclusion is supported by finite-element calculations performed by Mergel *et al.* [28] and more recently by Lengiewicz *et al.* [29] (see also [30] and [14]), which show that even without adhesion there is a reduction in the contact area between an elastic cylinder and a flat surface as a tangential force is applied to the cylinder.

V. SUMMARY AND CONCLUSION

In this article, we studied two aspects of adhesion that shed light on recent debates in contact mechanics (with adhesion) [6,26,31]. First, we discussed the adhesion paradox, the fact that adhesion is usually not observed at macroscopic length scales. We presented experimental results and theoretical calculations that showed that adhesion in most cases is "killed" by the long-wavelength part of the roughness spectrum. Secondly, the results of adhesion experiments between a human finger and a flat smooth glass surface were presented. We found that there was no macroscopic adhesion between these contacting pairs in the dry state. Based on this result, we suggest that the decrease in the contact area as reported in the literature [5,10,32] results from nonadhesive contact mechanics, involving large deformations of complex layered material.

ACKNOWLEDGMENTS

[1] K. Kendall, *Molecular Adhesion and Its Applications: The Sticky Universe* (Springer Science and Business Media, New York, 2007).

[2] B. N. J. Persson, On the mechanism of adhesion in biological systems, J. Chem. Phys. **118**, 7614 (2003).

[3] B. N. J. Persson, O. Albohr, U. Tartaglino, A. I. Volokitin, and E. Tosatti, On the nature of surface roughness with application to contact mechanics, sealing, rubber friction and adhesion, J. Phys.: Condens. Matter **17**, R1 (2004).

[4] L. Pastewka and M. O. Robbins, Contact between rough surfaces and a criterion for macroscopic adhesion, Proc. Natl. Acad. Sci. (USA) **111**, 3298 (2014).

[5] R. Sahli, G. Pallares, C. Ducottet, I. E. Ben Ali, S. A. Akhrass, M. Guibert, and J. Scheibert, Evolution of real contact area under shear and the value of static friction of soft materials, Proc. Natl. Acad. Sci. (USA) **115**, 471 (2018).

[6] M. Ciavarella, Universal features in stickiness criteria for soft adhesion with rough surfaces, Tribol. Int. **146**, 106031 (2020).

[7] M. H. Müser, A dimensionless measure for adhesion and effects of the range of adhesion in contacts of nominally flat surfaces, Tribol. Int. **100**, 41 (2016).

[8] A. Wang and M. H. Müser, Gauging Persson theory on adhesion, Tribol. Lett. **65**, 103 (2017).

[9] D. J. Meyer, M. A. Peshkin, and J. E. Colgate, *Fingertip Friction Modulation due to Electrostatic Attraction*, World Haptics Conference (WHC) (IEEE, Daejeon, South Korea, 2013), pp. 43–48.

[10] O. Sirin, A. Barrea, P. Lefevre, J. L. Thonnard, and C. Basdogan, Fingerpad contact evolution under electrovibration, J. R. Soc., Interface **16**, 20190166 (2019).

[11] E. L. Church and P. Z. Takacs, Optical testing and metrology III: Recent advances in industrial optical inspection, Proc. SPIE **1332**, 504 (1991).

[12] P. R. Nayak, Random process model of rough surfaces, J. Lubrication Technol. **93**, 398 (1971).

[13] G. Carbone, B. Lorenz, B. N. J. Persson, and A. Wohlers, Contact mechanics and rubber friction for randomly rough surfaces with anisotropic statistical properties, Eur. Phys. J. E **29**, 275 (2009).

[14] J. S. Persson, A. Tiwari, E. Valbahs, T. V. Tolpekina, and B. N. J. Persson, On the use of silicon rubber replica for surface topography studies, Tribol. Lett. **66**, 140 (2018).

[15] O. D. Gordan, B. N. J. Persson, C. M. Cesa, D. Mayer, B. Hoffmann, S. Dieluweit, and R. Merkel, On pattern transfer in replica molding, Langmuir **24**, 6636 (2008).

[16] B. N. J. Persson and E. Tosatti, The effect of surface roughness on the adhesion of elastic solids, J. Chem. Phys. **115**, 5597 (2001).

[17] L. Dorogin, A. Tiwari, C. Rotella, P. Mangiagalli, and B. N. J. Persson, Role of preload in adhesion of rough surfaces, Phys. Rev. Lett. **118**, 238001 (2017).

[18] S. Dalvi, A. Gujrati, S. R. Khanal, L. Pastewka, A. Dhinojwala, and T. D. B. Jacobs, Linking energy loss in soft adhesion to surface roughness, Proc. Natl. Acad. Sci. (USA) **116**, 25484 (2019).

[19] A. L. Barabasi and H. E. Stanley, *Fractal Concepts in Surface Growth Hardcover* (Cambridge University Press, Cambridge, 1995).

[20] B. N. J. Persson, On the fractal dimension of rough surfaces, Tribol. Lett. **54**, 99 (2014).

[21] A. Tiwari, L. Dorogin, A. I. Bennett, K. D. Schulze, W. G. Sawyer, M. Tahir, and B. N. J. Persson, The effect of surface roughness and viscoelasticity on rubber adhesion, Soft Matter **13**, 3602 (2017).

[22] L. Dorogin, A. Tiwari, C. Rotella, P. Mangiagalli, and B. N. J. Persson, Adhesion between rubber and glass in dry and lubricated condition, J. Chem. Phys., **148**, 234702 (2018).

[23] B. N. J. Persson, I. M. Sivebaek, V. N. Samoilov, K. Zhao, A. I. Volokitin, and Z. Zhang, On the origin of Amonton's friction law, J. Phys.: Condens. Matter **20**, 395006 (2008).

[24] B. N. J. Persson, Adhesion between an elastic body and a randomly rough hard surface, Eur. Phys. J. E **8**, 385 (2002).

[25] B. N. J. Persson and M. Scaraggi, Theory of adhesion: Role of surface roughness, J. Chem. Phys. **141**, 124701 (2014).

[26] A. Papangelo, J. Scheibert, R. Sahli, G. Pallares, and M. Ciavarella, Shear-induced contact area anisotropy explained by a fracture mechanics model, Phys. Rev. E **99**, 053005 (2019).

[27] H. Zahouania, S. Mezghanib, R. Vargiolua, T. Hoca, and M. EL Mansori, Effect of roughness on vibration of human finger during a friction test, Wear **301**, 343 (2013).

[28] J. C. Mergel, J. Scheibert, and R. A. Sauer, Contact with coupled adhesion and friction: Computational framework, applications, and new insights, arXiv:2001.06833.

[29] J. Lengiewicz, M. de Souza, M. Lahmar, C. Courbon, D. Dalmas, S. Stupkiewicz, and J. Scheibert, Finite deformations govern the anisotropic shear-induced area reduction of soft elastic contacts, J. Mech. Phys. Solids **143**, 104056 (2020).

[30] J. C. Mergel, R. Sahli, J. Scheibert, and R. A. Sauer, Continuum contact models for coupled adhesion and friction, T. J. Adhesion **95**, 1101 (2019).

[31] G. Violano, L. Afferrante, A. Papangelo, and M. Ciavarella, On stickiness of multiscale randomly rough surfaces, J. Adhesion **0**, 1(2019).

[32] R. Sahli, G. Pallares, A. Papangelo, M. Ciavarella, C. Ducottet, N. Ponthus, and J. Scheibert, Shear-Induced Anisotropy in Rough Elastomer Contact, Phys. Rev. Lett. **122**, 214301 (2019).